Radiation Measurements 174 (2024) 107108

Contents lists available at ScienceDirect

Radiation Measurements

journal homepage: www.elsevier.com/locate/radmeas

Quantitative assessment of signal and noise properties of mammography digital detectors

Alessandra Maia Marques Martinez Perez [a,*], Laura Alcantara Silva Lopes [a], Renato França Caron [b], Bruno Beraldo Oliveira [b], Linda Viola Ehlin Caldas [c], Martin Eduardo Poletti [a]

[a] Departamento de Física, FFCLRP, University of São Paulo, 14040-901, Ribeirão Preto, SP, Brazil
[b] Departamento de Prevenção, Barretos Cancer Hospital, 14784-400, Barretos, SP, Brazil
[c] Instituto de Pesquisas Energéticas e Nucleares, Comissão Nacional de Energia Nuclear, IPEN/CNEN, 05508-000, São Paulo, SP, Brazil

ARTICLE INFO

Keywords:
Digital mammography
Detector air kerma
Signal transfer property
Noise component analysis
Noise stationarity

ABSTRACT

Recent measurements introduced in quality control protocols indicate large variations in the evaluated parameters, pointing out as their main cause the different detectors used. The objective of this work was to characterize, in terms of signal transfer property (STP) and noise component analysis (NCA), six mammography digital detectors at different DAK levels for a variety of beam qualities. A Carestream EHR-M3 CR detector and Siemens Opdima, Planmed Clarity, GE Essential, GE Pristina and GE Crystal Nova DR detectors were characterized in terms of STP and NCA, as a function of detector air kerma (DAK) at the X-ray detector input plane. An extended DAK range was used. A PTW Unidos E electrometer with PTW Freiburg ionization chamber were used to measure DAK. Attenuated beam qualities (obtained by adding 2 mm Al to the corresponding beam qualities) used were 28 kV with anode/filter combination Mo/Mo for the EHR-M3, Opdima, Essential and Pristina detectors; 28 kV with W/Rh for the Crystal Nova; and 28 kV with W/Ag for the Clarity. To study the influence of beam quality, 28 kV with Mo/Rh and 34 kV with Rh/Ag were also used for EHR-M3 and Pristina, respectively. STP measures the relationship between the input (DAK) and the output (pixel value) detector signals. NCA gives the fraction of total noise of each of its components and was calculated from the variance in mean pixel value. Noise stationarity was evaluated using maps of standard deviation across the image plane. Parameters were determined under stipulated (geometric and irradiation) conditions given in EUREF quality control protocol. Computed radiography (CR) detector showed a logarithmic response and digital radiography (DR) detectors showed a linear response in the tested DAK range ($R^2 > 0.999$). For the DR detectors, the response function was also influenced by the beam quality, with a higher slope for more energetic beams. NCA showed that Opdima and EHR-M3 detectors are quantum limited below 290 μGy and 650 μGy, respectively. For higher DAK values, structure noise is the dominant noise source. All other detectors are quantum limited in the evaluated DAK range. Noise as a function of position in the image showed limited noise stationarity. The findings show that the signal transfer and noise characteristics are influenced by the properties of the detection system. Moreover, STP was influenced by the beam quality. NCA showed the influence of electronic and structure noise at lower and higher DAK, respectively. These results are useful for detector characterization.

1. Introduction

Image quality in mammograms is crucial for early detection, which can improve the prospects of cure of the disease (Ginsburg et al., 2020). High quality cancer screening and diagnosis are based on the implementation of quality assurance programs (Feigin, 2023). EUREF protocol (van Engen et al., 2013) establishes standards, protocols, and best practice recommendations in quality assurance of digital mammography systems. This protocol presents tests for systems using both computed radiography (CR) and digital radiography (DR) detectors. Though less dose efficient, CR detectors are still largely used in mammography screening, especially in developing countries, because

* Corresponding author.
E-mail address: alessamm@alumni.usp.br (A.M.M.M. Perez).

https://doi.org/10.1016/j.radmeas.2024.107108
Received 31 January 2024; Received in revised form 8 March 2024; Accepted 2 April 2024
Available online 8 April 2024

they represent a cost saving way for getting digital images (Diffey, 2015).

With the advent of digital detectors, most of detector dose limitations was overcome. Instead of film darkening, image quality is described by signal to noise ratio (SNR). However, the SNR can be improved almost arbitrarily by increasing the number of detected X-ray photons, which would increase patient radiation dose (Knight, 2020). A critical factor determining both image quality and dose is the spectral composition of the X-ray beam (Cunha et al., 2013). Due to the potential of dose reduction, especially for thicker breasts, newer systems employ more energetic X-ray beams, which may impact detector signal and noise (Borg et al., 2012; Alkhalifah et al., 2020).

With the rapid technological development, new detectors have been introduced on the market. Besides, existing detectors have been constantly updated. The study of signal and noise properties of an imaging detector is important in acceptance and constancy testing, optimization studies and detector characterization (Marshall et al., 2016; Gennaro et al., 2018; NHS. NHS Breast Screening Programme equipment report, 2019a, 2019b, 2019c, 2019d). Detector characterization involves measurements of signal and noise both in spatial and frequency domains. The study of signal and noise in frequency domain in terms of modulation transfer function (MTF), normalized noise power spectrum (NNPS) and detective quantum efficiency (DQE) is based on the use of linear-systems theory, which presupposes signal linearity and noise stationarity (Cunningham, 2000; ICRU, 2009).

Signal transfer property (STP) is a measure of signal linearity and relates input signal, in terms of detector air kerma (DAK), with the output signal in the image, given in terms of pixel value (PV) (ICRU, 2009). In a digital X-ray imaging detector, there are three main noise sources: electronic, quantum and structure. Noise component analysis (NCA) evaluates noise composition as a function of DAK and enables the identification of the quantum limited interval (Monnin et al., 2014).

Signal and noise properties in terms of STP and NCA of different digital detector technologies have been extensively investigated with different methodological approaches. In the early study of Ghetti et al. (2008), GE DS and GE Essential detectors were evaluated and the later one exhibited lower mean signal level and electronic noise for the same DAK level. Monnin and Verdun (2009) compared two digital mammography CR detectors: CR 975 with EHR-M2 and EHR-M3 plates. EHR-M3 was 33% more sensitive than the EHR-M2 and presented lower structure noise, which resulted in a reduction of 25% in total noise level. In a paper by Marshall (2009b) response function was measured as a function of energy for two full-field digital mammography systems, GE Senographe and Lorad Selenia, and an increase in STP gradient with mean X-ray energy was observed. Posteriorly, Marshall et al. (2011) have investigated 11 digital mammography detectors, based on CR and DR detectors. In this study, Carestream EHR-M3 and GE Essential were evaluated. Noise components and spatial stationarity of noise were assessed for different mammography systems by Monnin et al. (2014). Their results pointed out the limited stationarity of noise. Marshall et al. (2016) measured STP and NCA of a retrofit digital detector-based mammography system for three anode/filter settings and an estimated quantum noise limited range was given. England's National Health Service (NHS) has published several reports on technical evaluation of current mammography detectors, including GE Pristina (NHS. NHS Breast Screening Programme equipment report, 2019a, 2019b, 2019c, 2019d).

The use of linear-systems theory for detector characterization presupposes signal linearity and noise stationarity. There are few studies on noise stationarity, a basic requisite in NNPS analysis. Most literature works evaluated signal and noise characteristics in a narrow range of 10–800 μGy. Moreover, comparison of data is difficult, due to the different protocols adopted. In this study, signal linearity and noise stationarity have been studied using EUREF protocol. An extended DAK interval was used to better explore the influence of electronic and structure noise in lower and higher DAK levels, respectively.

The objective of this paper is to quantitatively assess signal linearity in terms of STP, noise in terms of NCA and noise stationarity of six digital mammography detectors in the spatial domain, for different beam qualities, using the European Guidelines protocol.

2. Material and methods

2.1. Evaluated detectors

Six digital mammography detectors were evaluated in this study: one computed radiography (CR) detector and five indirect conversion digital radiography (DR) units. The principal characteristics of the evaluated detectors are given in Table 1. The Carestream EHR-M3 plate was used with a DirectView CR 975 reader. Siemens Opdima is a small field digital mammography system, while the other DR units are full field digital mammography systems. Signal transfer property (STP) and noise component analysis (NCA) were assessed according to EUREF protocol (van Engen et al., 2013).

2.2. Beam characterization

The first step in the estimation of objective image quality parameters was the beam characterization. There was no common anode/filter combination available between the five X-ray units used. Therefore, a common beam energy could not be selected. For comparison purposes, we chose a common tube potential of 28 kV. In addition, to evaluate the influence of beam quality (kV and anode/filter combination), two different beam conditions were used for EHR-M3 and Pristina systems. An additional filtration of 2 mm Al was placed at the X-ray tube exit and the compression plate was removed from the beam (van Engen et al., 2013). Half value layer and air kerma were measured using PTW Unidos E electrometer with a TN34069 SFD mammo ionization chamber, calibrated for attenuated beam qualities. The ionization chamber was placed at approximately 4 cm above the bucky to reduce backscattered radiation from the bucky, 6 cm from the chest wall edge and laterally centralized. Detector air kerma (DAK) at the X-ray detector input plane was calculated applying an inverse square law correction.

2.3. Images acquisition

Flood images were acquired with the antiscatter grid removed from the beam, except for the Planmed Clarity detector. In the case of the Carestream EHR-M3, the cassette was placed on the bucky. For all detectors, images were acquired using the different beam qualities listed in Table 1, for the DAK values previously measured, with the system under manual control. Detectors were fully irradiated (open collimation) for image acquisitions. "For processing" images were used for all measurements. Pixel value (PV) and standard deviation (σ) were measured using ImageJ software at a ROI of 5 mm × 5 mm placed 60 mm from the chest wall edge and centered left–right on the detector (van Engen et al., 2013). STP and NCA calculations were performed using OriginPro 2021 software (Seifert, 2014). There are software products for quantitative assessment of STP and NCA in digital mammography (Marshall, 2009a; Porzio and Konstantinidis, 2021). We validated our results against well-established software used in mammography Mammo_QC (Porzio and Konstantinidis, 2021) and found excellent agreement.

2.4. Signal transfer property (STP)

The signal transfer property (STP) describes the relationship between pixel value (PV) and DAK. The PV data were plotted against DA*K* and one of two curves fitted to the data:

$$\mathrm{PV} = A \cdot \mathrm{DA}K + B \tag{1}$$

or

Table 1
Characteristics of the X-ray detectors evaluated in this study along with acquisition factors used for the evaluation.

Manufacturer	Model	Del size (μm)	Detector dimensions (cm × cm)	Image matrix size	Technology	Tube potential anode/filter	HVL[a] (mm Al)	DAK range (μGy)
Carestream	EHR-M3[b]	48.5	18 × 24	3584 × 4784	BaFBr:Eu	28 kV Mo/Mo 28 kV Mo/Rh	0.56 0.62	8.7–1147 8.7–1323
Siemens	Opdima	48.5	4.9 × 8.6	1024 × 1792	CsI/CCD	28 kV Mo/Mo	0.56	8.7–376
Planmed	Clarity	83	23.2 × 29.7	2796 × 3584	CsI/aSi/TFT	28 kV W/Ag	0.89	27–999
GE	Essential	100	23.9 × 30.6	2394 × 3062	CsI/aSi/TFT	28 kV Mo/Mo	0.57	24–1575
GE	Pristina	100	23.9 × 28.5	2394 × 2850	CsI/aSi/TFT	28 kV Mo/Mo 34 kV Rh/Ag	0.58 0.93	23–720 70–844
GE	Crystal Nova	100	17.8 × 23.4	1780 × 2340	CsI/aSi/TFT	28 kV W/Rh	0.75	4–1573

[a] Attenuated beam.
[b] It was used with a Siemens Mammomat 3000Nova X-ray tube.

$$PV = A \cdot \mathrm{Log}(DAK) + B \quad (2)$$

where A and B are the fit coefficients.

For non-linear detectors, the inverse of STP was used to convert all image data to DAK on a pixel-wise basis before noise analysis. This step linearized the image PV data, removed any offset that was present and gave images of unity gain (van Engen et al., 2013).

2.5. Noise component analysis (NCA)

The standard deviation data were used to perform a basic separation of detector noise sources based on a polynomial model for image variance. The variance in the image was assumed to follow the relationship (Hillen et al., 1987; Marshall et al., 2011; van Engen et al., 2013)

$$\sigma^2 = k_e + k_q \cdot DAK + k_s \cdot DAK^2 \quad (3)$$

where the first term represents electronic noise, the second one accounts for quantum (X-ray photon) noise and the third one refers to structured noise. The polynomial model assumes that electronic noise is an additive source and therefore is independent of DAK (Siewerdsen et al., 1997). Quantum noise variance scales with DAK (at a fixed beam quality and assuming Poisson noise) (Rimkus and Baily 1983). Structured noise results from factors such as spatial gain variations of the X-ray convertor layer, large area nonuniformity from the X-ray beam (heel effect), scratches on the detector cover, dust and any non-uniformity added by the detector corrections (Burgess, 2004; Marshall et al., 2011). The variance from these factors is amplified by the X-ray signal used, and it is a multiplicative source.

For a given detector, standard deviation was taken from the flood image using the reference ROI, and variance was plotted as a function of DAK. To evaluate the influence of structure noise high values of DAK (up to 1600 μGy) were used. Experimental data were fitted to equation (3) using a weighted least-square method and the coefficients k_e, k_q and k_s were determined (van Engen et al., 2013).

The quantum limited range is defined as the exposure range in which the quantum noise component is greater than the electronic or structure noise components. Using the polynomial decomposition method, the limits of quantum limited range can be easily calculated from the ratios between noise coefficients (Monnin et al., 2014).:

$$\frac{k_e}{k_q} < DAK < \frac{k_q}{k_s} \quad (4)$$

Another model was used for noise analysis. It consists of an allometric adjustment of standard deviation plotted as a function of DAK (Marshall et al., 2011). An equation of the form

$$\sigma = a \cdot DAK^b \quad (5)$$

was fitted to the data; if image noise consists of pure quantum (X-ray) noise across the exposure range examined, then a coefficient b equal to 0.5 is expected. The presence of the additive and multiplicative detector noise sources discussed above will cause coefficient b to deviate from 0.5 (Marshall et al., 2011).

2.6. Noise stationarity

First, the images were de-trended using a 2D second-order polynomial function. Then, spatial stationarity of noise was measured by calculating noise maps across the imaging plane using 5 × 5 mm^2 ROI. For the sake of comparison between the detectors, the standard deviation was normalized by the standard deviation measured in EUREF reference ROI (Monnin et al., 2014).

3. Results and discussion

3.1. Signal transfer property (STP)

Fig. 1(a) presents the STP for the three DR detectors using Mo/Mo anode/filter combination. STP for two DR detectors using W anode and filters of Rh and Ag are plotted in Fig. 1(b). Fig. 1(c) and (d) show the STP for two anode/filter settings for the Pristina and the EHR-M3 detectors, respectively. The associated fit coefficients are listed in Table 2.

Fig. 1(a) shows that STP was similar for the different detectors using the same anode/filter combination Mo/Mo. In Fig. 1(b)–(c) an increase in signal for more energetic beams for DR detectors is observed. An increase in STP slope for the detector using W/Ag when compared to W/Rh is seen in Fig. 1(b). Fig. 1(c) shows that GE Pristina exhibits higher STP slope for the Rh/Ag beam when compared to Mo/Mo. These findings indicate that the beam energy (HVL) influences STP for DR detectors, with an increase in signal for more energetic beams. This behavior may be related to a few factors. First, as beam energy increases there is an increase in the number of X-ray photons per unit air kerma. Besides, more energetic photons can generate a greater number of secondary quanta. In addition, as beam energy increases, the X-ray interaction occurs deeper in the phosphor. Since flat panel detectors are read out by the light sensitive pixel array positioned at the exit surface of the converter, layer depth/site of light photon production moves closer to the pixel array, which increases secondary carrier collection efficiency (Marshall, 2009b). These effects combined result in higher signal values with increasing beam energy.

By way of contrast, in Fig. 1(d) STP presented no beam energy dependence for the EHR-M3 detector. A possible explanation was given by Marshall et al. (2017) in a study using CR detectors for paediatric radiography applications. Though the number of X-ray photons and secondary photons increase with X-ray energy, this signal is generated deeper within the plate during readout. The fact that photostimulable signal is read from the top surface of CR plate implies an increase in the

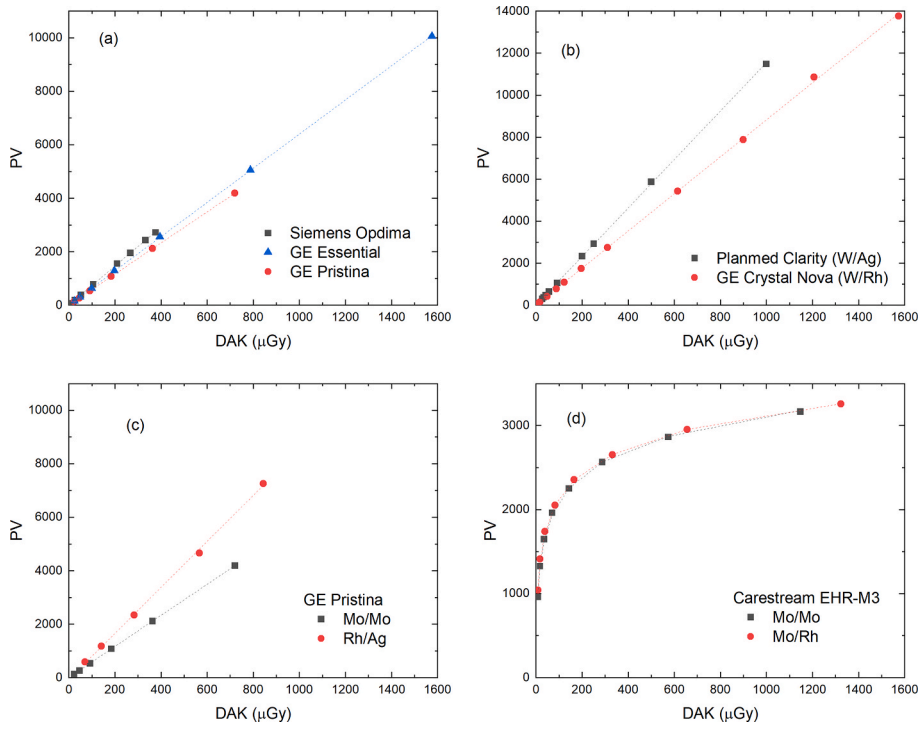

Fig. 1. PV plotted as a function of DAK for (a) three DR mammography detectors using Mo/Mo anode/filter combination and (b) two DR detectors using W anode (Rh and Ag filters); (c) GE Pristina detector using Mo/Mo and Rh/Ag beam qualities and (d) Carestream EHR-M3 detector using Mo/Mo and Mo/Rh. Filled symbols for experimental data and dashed lines for fitted curves. Uncertainties are smaller than data symbols.

Table 2
STP type and fit coefficients.

Detector	Anode/filter[a]	STP	A	B
EHR-M3	Mo/Mo	Logarithmic	1025 ± 13	44 ± 28
	Mo/Rh	Logarithmic	1004 ± 8	126 ± 17
Opdima	Mo/Mo	Linear	7.28 ± 0.04	11 ± 9
Clarity	W/Ag	Linear	11.54 ± 0.05	13 ± 19
Essential	Mo/Mo	Linear	6.39 ± 0.01	8 ± 8
Pristina	Mo/Mo	Linear	5.819 ± 0.008	1 ± 3
	Rh/Ag	Linear	8.6 ± 0.2	−64 ± 73
Crystal Nova	W/Rh	Linear	8.82 ± 0.04	6 ± 30

[a] Additional filtration of 2 mm Al.

distance that stimulated photons must travel, resulting in greater losses and signal reduction. These effects counterbalance each other and no difference in signal levels is observed.

The evaluated detectors were found to have the expected relationship between detector air kerma (DAK) and pixel values (PV), i.e., logarithmic for the Carestream EHR-M3 CR detector (Monnin and Verdun, 2009; Marshall et al., 2011) and linear for the DR detectors (Ghetti et al., 2008; Marshall et al., 2011; NHS. NHS Breast Screening Programme equipment report, 2019d). For EHR-M3 detector, sensitivity was up to 30% lower when compared to data from Monnin and Verdun (2009). This may be related to the different CR readers used. From values in Tables 2 and it is noted that the five indirect DR detectors evaluated were calibrated with different gain and offset. Data for the Essential detector was in close agreement with those obtained by Ghetti et al. (2008), while data from Marshall et al. (2011) were up to 19% higher, due to the use of a more energetic beam quality (Rh/Rh). PV up to 24% lower values were obtained for the Pristina detector when compared to NHS (NHS. NHS Breast Screening Programme equipment report, 2019d). This may be associated with the different protocol adopted for data acquisition and analysis (Kulama et al., 2009).

The measurement of STP is required for quantitative analysis in terms of MTF and NNPS (van Engen et al., 2013). The MTF describes the spatial frequency response of a detector and is typically determined using an edge placed at the detector input plane (van Engen et al., 2013). The NNPS describes the variance of an image intensity divided among its frequency components and is calculated from ROIs taken from a region of a flood image (van Engen et al., 2013). STP results obtained are useful to linearize edge and flood images prior to MTF and NNPS calculations.

3.2. Noise component analysis (NCA)

The fitting coefficients for the polynomial and allometric noise models, as well as the estimated DAK (lower and upper) where quantum noise is no longer the dominant noise component, are given in Table 3. Variance for the three noise sources expressed as a fraction of total variance is plotted in Fig. 2(a)-(e).

From the noise model in Equation (3), electronic noise dominates at low DAK, while structured noise becomes increasingly important at high DAK. At the lowest DAK studied, electronic noise accounted for 20% of total noise variance for the Siemens Opdima and Planmed Clarity detectors, 30% for the Carestream EHR-M3 and GE Crystal Nova and 40% for the Pristina detector. For the GE Essential, electronic noise coefficient presented a negative value. The reason is that the electronic noise has a different DAK dependency than assumed by the polynomial model. As appointed by Monnin et al. (2014), negative coefficients can provide information on whether the three-component model is suitable or valid for a given detector. From Fig. 2(a)–(e), it is seen that all the detectors were quantum noise limited in the DAK range studied, except for the Opdima and EHR-M3, which are quantum limited below ~290 μGy and ~650 μGy, respectively. These values are in close agreement with estimated upper DAK limit in Table 3. An imaging system is called quantum limited when the quality of the recorded image (signal-to-noise ratio) is primarily defined by the statistics of the incoming quantum fluence. The range of quantum limited operation can be regarded as the working space where the quantum utilization is reasonably high (Hillen et al., 1987). A well-designed detector is expected to be quantum limited for all DAK values used clinically (Marshall et al., 2011).

Table 3
Coefficients determined from noise component analysis using polynomial and allometric models; approximate DAK (lower and upper) where quantum noise is no longer the dominant noise component.

Detector	Anode/ filter	k_e	k_q	k_s	Lower DAK limit (μGy)	Upper DAK limit (μGy)	b
EHR-M3	Mo/Mo	0.09 ± 0.06	0.0221 ± 0.0004	(3.48 ± 0.04) × 10^{-5}	4	635	0.68 ± 0.03
	Mo/Rh	0.14 ± 0.11	0.0181 ± 0.0006	(4.91 ± 0.05) × 10^{-5}	8	368	0.76 ± 0.03
Opdima	Mo/Mo	2 ± 6	1.10 ± 0.08	(3.8 ± 0.2) × 10^{-3}	2	289	0.66 ± 0.03
Clarity	W/Ag	9 ± 12	1.64 ± 0.09	(6.3 ± 0.9) × 10^{-4}	5	2603	0.54 ± 0.02
Essential	Mo/Mo	−16 ± 7	0.76 ± 0.06	(4 ± 7) × 10^{-5}	–	–	0.58 ± 0.02
Pristina	Mo/Mo	3.4 ± 0.8	0.195 ± 0.007	(6.2 ± 0.9) × 10^{-5}	17	3145	0.49 ± 0.02
	Rh/Ag	4.0 ± 0.9	0.328 ± 0.006	(1.23 ± 0.06) × 10^{-4}	12	2667	0.54 ± 0.01
Crystal Nova	W/Rh	0.5 ± 3	0.29 ± 0.02	(8 ± 1) × 10^{-5}	2	3625	0.55 ± 0.02

For higher values of DAK for the Opdima and EHR-M3, structure noise is dominant. For the Opdima detector, structure noise is related to the presence of wide range inhomogeneities in the data, while for CR detectors, it is related to the phosphor grain size (Thunberg et al., 1999 ; Rowlands, 2002).

Table 3 presents the fitted b coefficients for Equation (5) for the different detectors. This table shows higher b coefficients for the EHR-M3 and Opdima detectors (b > 0.6), where structure noise forms a higher proportion of detector noise. Coefficients for the other detectors are close to 0.5, ranging from 0.4 to 0.6; quantum noise remained the dominant noise source for these detectors over the DAK range studied.

From DAK limits in Tables 3 and it is seen that quantum noise limited range was narrower for the more energetic beam qualities used for EHR-M3 and Pristina systems. This finding is consistent with the higher values of b coefficient for these beam qualities, related to an increased contribution of structure noise.

A value of 0.58 was obtained for the Essential detector, compared to 0.46 estimated from Ghetti et al. (2008) and 0.49 given by Marshall et al. (2011). Measurements in this study were accomplished in an aged equipment, whose scratches on the detector cover gave rise to structure noise, increasing coefficient b. For EHR-M3 detector, b coefficient was 0.68 compared to the value 0.61 reported by Marshall et al. (2011). Value of the coefficient b obtained in this study for the EHR-M3 was higher due to the wider DAK range employed. For higher DAK values, structure noise forms a higher proportion of detector noise, causing b coefficient to increase. Upon using a narrower DAK interval, the new value of b obtained was the same as the one reported by Marshall et al. (2011). For the Pristina detector, on the other hand, the same value of 0.54 was obtained in this study and in NHS report (NHS. NHS Breast Screening Programme equipment report, 2019d), reflecting the similar DAK range adopted.

3.3. Noise stationarity

Fig. 2(f) shows the standard deviation profile across the mid-line of the detector as a function of distance to chest wall edge for the GE Essential, GE Pristina and GE Crystal Nova detectors for a target DAK of 100 μGy. The noise is not constant over the image plane, with higher levels at the periphery of the image plane. Noise generally increases from the chest wall side to the nipple side. For the systems Essential and Pristina, the ratio in standard deviation between the areas of highest and lowest noise in the image reaches a factor of approximately 2. The central area of the detector, which is usually covered by the breast and includes the ROI recommended by EUREF protocol, is close to the average noise level of the image. EUREF states that a ROI of 100 mm × 100 mm can be used for NNPS estimation. Though noise is not globally stationary across the image plane, Fig. 2(f) shows that it presents local invariance in this area, where the variation in standard deviation is inferior to 20%. On the other hand, IEC 62220-1-2 (IEC. International Electrotechnical Commission, 2007) defines an area of 50 mm × 50 mm. This strictly limits the physical region from which NNPS is calculated, reducing the effects of non-stationarity, however several images are required to reduce uncertainty of spectral estimate. Our results show that the use of a 50 mm × 50 mm ROI instead of 100 mm × 100 mm would reduce variation in standard deviation by 5% for the Essential, while for Pristina and Crystal Nova a reduction of only 2% would be achieved. More studies are necessary to verify if stationarity conditions are fulfilled. However, noise distribution for the GE Essential is close to the reported by Monnin et al. (2014) for the same detector.

4. Conclusions

This study has assessed, in accordance with the European Guidelines protocol, the signal and noise properties (STP and NCA) of six digital mammography detectors, at different detector air kerma (DAK) levels for a variety of beam qualities. The STP of the CR detector EHR-M3 exhibited no dependence on beam energy, while for the DR detectors sensitivity in terms of STP was higher for more energetic beams. STP results obtained are useful to linearize edge and flood images prior to MTF and NNPS calculations. All the evaluated detectors were quantum limited in the DAK range used, except Opdima and EHR-M3, which were quantum limited for DAK values inferior to 290 μGy and 650 μGy, respectively. Structure noise is the dominant noise source for higher DAK values, suggesting that the use of higher DAK values has implications not only in patient dose, but in reducing image quality as well. The noise stationarity analysis showed that noise may differ from one location to another across the image plane. These results provide an insight on noise stationarity, a basic requisite in NNPS analysis.

The authors declare that they have no conflict of interest.

CRediT authorship contribution statement

Alessandra Maia Marques Martinez Perez: Project administration, Methodology, Formal analysis, Conceptualization, Data curation, Investigation, Validation, Visualization, Writing – original draft. **Laura Alcantara Silva Lopes:** Data curation, Investigation, Validation. **Renato França Caron:** Resources. **Bruno Beraldo Oliveira:** Resources. **Linda Viola Ehlin Caldas:** Visualization. **Martin Eduardo Poletti:** Writing – review & editing, Visualization, Conceptualization, Funding acquisition, Investigation, Project administration, Resources, Supervision, Validation.

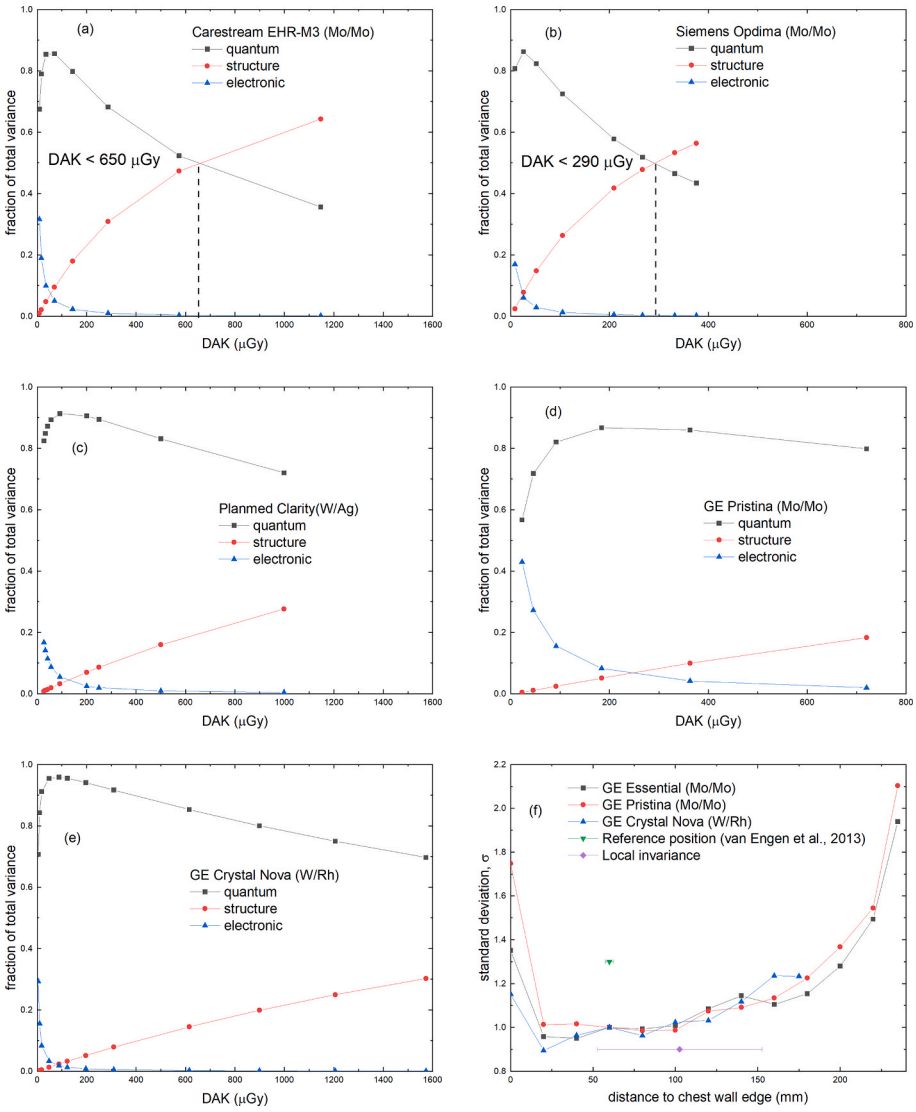

Fig. 2. Electronic, quantum and structured noise variance presented as a fraction of total noise variance for (a) Carestream EHR-M3, (b) Siemens Opdima, (c) Planmed Clarity, (d) GE Pristina and (e) GE Crystal Nova detectors; (f) Standard deviation as a function of distance to chest wall edge for the detectors GE Essential (Mo/Mo), GE Pristina (Mo/Mo) and GE Crystal Nova (W/Rh). Dashed lines indicate DAK limit for quantum noise limited behavior.

Declaration of competing interest

The authors declare that they have no known competing financial interests or personal relationships that could have appeared to influence the work reported in this paper.

Data availability

Data will be made available on request.

Acknowledgments

This study was financed in part by the Coordenação de Aperfeiçoamento de Pessoal de Nível Superior - Brasil (CAPES) - Finance Code 001; and the Conselho Nacional de Desenvolvimento Científico e Tecnológico (CNPq) under grants N° 312643/2018-7, N° 311710/2022-0 and N° 305142/2021-6.

References

Alkhalifah, K., Asbeutah, A., Brindhaban, A., 2020. Image quality and radiation dose for fibrofatty breast using target/filter combinations in two digital mammography systems. J.Clin.Imag.Sci. 10, 56. https://doi.org/10.25259/JCIS_30_2020.

Borg, M., Badr, I., Royle, G.J., 2012. The use of a figure-of-merit (FOM) for optimisation in digital mammography: a literature review. Radiat. Protect. Dosim. 151 (1), 81–88. https://doi.org/10.1093/rpd/ncr465.

Burgess, A., 2004. On the noise variance of a digital mammography system. Med. Phys. 31, 1987–1995.

Cunha, D.M., Tomal, A., Poletti, M.E., 2013. Monte Carlo simulation of X-ray spectra in mammography and contrast-enhanced digital mammography using the Code PENELOPE. IEEE Trans. Nucl. Sci. 2, 495–502. https://doi.org/10.1109/TNS.2012.2226750.

Cunningham, I.A., 2000. Applied linear-systems theory. In: Van Metter, R.L., Beutel, J., Kundel, H.L. (Eds.), Physics and Physicophysics, Belligham: SPIE, vol. 1, pp. 81–159.

Diffey, J.L., 2015. A comparison of digital mammography detectors and emerging technology. Radiography 21 (4), 315–323. https://doi.org/10.1016/j.radi.2015.06.007.

Feigin, K., 2023. Quality assurance in Mammography: an overview. Eur. J. Radiol. 165, 110935 https://doi.org/10.1016/j.ejrad.2023.110935.

Gennaro, G., Avramova-Cholakova, S., Azzalini, A., Luisa Chapel, M., Chevalier, M., Ciraj, O., de Las Heras, H., Gershan, V., Hemdal, B., Keavey, E., Lanconelli, N., Menhart, S., João Fartaria, M., Pascoal, A., Pedersen, K., Rivetti, S., Rossetti, V., Semturs, F., Sharp, P., Torresin, A., 2018. Quality controls in digital mammography protocol of the EFOMP mammo working group. Phys. Med. 48, 55–64. https://doi.org/10.1016/j.ejmp.2018.03.016.

Ghetti, C., et al., 2008. Physical characteristics of GE Senographe Essential and DS digital mammography detectors. Med. Phys. 35 (2), 456–463. https://doi.org/10.1118/1.2828185.

Ginsburg, O., Yip, C.H., Brooks, A., Cabanes, A., Caleffi, M., Dunstan Yataco, J.A., Gyawali, B., McCormack, V., McLaughlin de Anderson, M., Mehrotra, R., Mohar, A., Murillo, R., Pace, L.E., Paskett, E.D., Romanoff, A., Rositch, A.F., Scheel, J.R., Schneidman, M., Unger-Saldaña, K., Vanderpuye, V., Wu, T.Y., Yuma, S., Dvaladze, A., Duggan, C., Anderson, B.O., 2020. Breast cancer early detection: a phased approach to implementation. Cancer 126 (Suppl. 10), 2379–2393. https://doi.org/10.1002/cncr.32887. Suppl 10.

Hillen, W., Schiebel, U., Zaengel, T., 1987. Imaging performance of a digital storage phosphor system. Med. Phys. 14, 744–751.

ICRU, 2009. International commission on radiation units and measurements. ICRU Report 82. Mammography – Assessment of Image Quality. Maryland.

IEC. International Electrotechnical Commission, 2007. Medical Electrical Equipment – Characteristics of Digital X-Ray Image Devices – Part 1-2: Determination of the Detective Quantum Efficiency - Detectors Used in Mammography. Geneva.

Knight, S.P., 2020. Contemporary research in digital radiography. J. Med. Radiat. Sci. 4, 254–256. https://doi.org/10.1002/jmrs.437.

Kulama, E., Burch, A., Castellano, I., et al., 2009. Commissioning and Routine Testing of Full Field Digital Mammography Systems (NHSBSP Equipment Report 0604. NHS Cancer Screening Programmes, Sheffield, Version 3.

Marshall, N.W., 2009a. Calculation of Quantitative Image Quality Parameters Notes Describing the Use of OBJ_IQ_reduced (NHSBSP Equipment Report 0902). NHS Cancer Screening Programmes, Sheffield.

Marshall, N.W., 2009b. Detective quantum efficiency measured as a function of energy for two full-field digital mammography systems. Phys. Med. Biol. 54 (9), 2845.

Marshall, N.W., et al., 2011. Image quality assessment in digital mammography: part I. Technical characterization of systems. Phys. Med. Biol. 56, 4201–4220.

Marshall, N.W., van Ongeval, C., Bosmans, H., 2016. Performance evaluation of a retrofit digital detector-based mammography system. Phys. Med. 32, 312–322.

Marshall, N.W., et al., 2017. Technical characterization of five x-ray detectors for paediatric radiography applications. Phys. Med. Biol. 62 (24), N573.

Monnin, P., Verdun, F.R., 2009. Qualification of Digital Mammography Imaging Systems Kodak CR 975 – EHR-M2 & EHR-M3. Institut Universitaire de Radiophysique Appliquée, Lausanne.

Monnin, P., et al., 2014. Comparison of the polynomial model against explicit measurements of noise components for different mammography systems. Phys. Med. Biol. 59, 5741. https://doi.org/10.1088/0031-9155/59/19/5741.

NHS. NHS Breast Screening Programme equipment report, 2019a. Technical Evaluation of Siemens Revelation Digital Mammography System in 2D Mode. Public Health England, London.

NHS. NHS Breast Screening Programme equipment report, 2019b. Technical Evaluation of Hologic 3Dimensions Digital Mammography System in 2D Mode. Public Health England, London.

NHS. NHS Breast Screening Programme equipment report, 2019c. Technical Evaluation of IMS Giotto Class Digital Mammography System in 2D Mode. Public Health England, London.

NHS. NHS Breast Screening Programme equipment report, 2019d. Technical Evaluation of GE Senographe Pristina Digital Mammography System in 2D Mode. Public Health England, London.

Porzio, M., Konstantinidis, A., 2021. Mammo_QC: free software for quality control (QC) analysis in digital mammography and digital breast tomosynthesis compliant with the European guidelines and EUREF/EFOMP protocols. Biomedical Physics & Engineering Biomed.Phys.Eng. Express 7 (6). https://doi.org/10.1088/2057-1976/ac2076.

Rimkus, D., Baily, N.A., 1983. Quantum noise in detectors. Med. Phys. 10, 470–471.

Rowlands, J.A., 2002. The physics of computed radiography. Phys. Med. Biol. 47, R123–R166.

Seifert, E., 2014. Origin pro 9.1: scientific data analysis and graphing software-software review. J. Chem. Inf. Model. 54 (5), 1552. https://doi.org/10.1021/ci500161d.

Siewerdsen, J.H., Antonuk, L.E., el-Mohri, Y., Yorkston, J., Huang, W., Boudry, J.M., Cunningham, I.A., 1997. Empirical and theoretical investigation of the noise performance of indirect detection, active matrix flat-panel imagers (AMFPIs) for diagnostic radiology. Med. Phys. 24, 71–89.

Thunberg SJ, et al. OPDIMA: large-area CCD-based x-ray image sensor for spot imaging and biopsy control in mammography. Medical Imaging 1999: Phys. of Medical Imaging; 3659: 150-158. doi 10.1117/12.349488..

van Engen, R., Bosmans, H., Dance, D., et al., 2013. Digital mammography update: European protocol for the quality control of the physical and technical aspects of mammography screening. In: European Guidelines for Quality Assurance in Breast Cancer Screening and Diagnosis, fourth ed. – Supplements. European Commission, Luxembourg.